HHS Public Access

Author manuscript

Radiother Oncol. Author manuscript; available in PMC 2017 January 01.

Published in final edited form as:

Radiother Oncol. 2016 January ; 118(1): 72–78. doi:10.1016/j.radonc.2015.11.018.

[18F]FLUORO-2-DEOXY-2-D-GLUCOSE VERSUS 3′-DEOXY-3′-[18F]FLUOROTHYMIDINE FOR DEFINING HEMATOPOIETICALLY ACTIVE PELVIC BONE MARROW IN GYNECOLOGIC PATIENTS

Jeffrey C. Wyss, J.D.[1], **Ruben Carmona, M.D., M.A.S.**[1], **Roshan A. Karunamuni, Ph.D.**[1], **Jakub Pritz, Ph.D.**[1], **Carl K. Hoh, M.D.**[2], and **Loren K. Mell, M.D.**[1]

[1]Department of Radiation Medicine and Applied Sciences, University of California San Diego, La Jolla, CA

[2]Department of Radiology, Division of Nuclear Medicine, University of California San Diego, La Jolla, CA

Abstract

Background and Purpose—We compared [18F]fluoro-2-deoxy-2-D-glucose (FDG) versus 3′-deoxy-3′-[18F]fluorothymidine (FLT) for the purpose of identifying active pelvic bone marrow (BM), quantifying its locational variation, and determining which technique is likely to be better for BM-sparing radiation planning.

Material and Methods—We sampled 41 patients, of which 25 underwent FDG-PET/CT only, 7 underwent FLT-PET/CT only, and 9 underwent both. Active BM subvolumes were defined as subsets of the pelvic BM with the highest standardized uptake values comprising 40%, 50%, and 60% of the total pelvic BM volume. We used the Dice similarity coefficient to quantify the percent overlap of active BM volumes of equal size. Differences in the spatial distribution of active BM were assessed using a region-growing algorithm.

Results—For patients with both modalities, the mean Dice coefficients for the 40%, 50%, and 60% subvolumes were 0.683, 0.732, and 0.781 respectively. Comparing individual active BM subvolumes to the mean subvolume, Dice coefficients varied from 0.598–0.889 for FDG and 0.739–0.912 for FLT. Region growing analysis showed FLT-PET defined more highly clustered active BM subvolumes.

Conclusions—Within the limitations of a small sample size, we found significant agreement between FDG-PET and FLT-PET; however, FLT-PET had significantly less individual variation and is likely to be superior to FDG-PET for BM-sparing radiotherapy.

Corresponding Author: Loren K. Mell, M.D., Associate Professor, Department of Radiation Medicine and Applied Sciences, 3855 Health Sciences Drive, MC0843, La Jolla, CA 92093, lmell@ucsd.edu / +1-858-246-0471/ fax +1-858-822-5568.

CONFLICT OF INTEREST STATEMENT

No potential conflict of interests.

Keywords

^{18}F-FDG; ^{18}F-FLT; active bone marrow; radiotherapy planning

INTRODUCTION

Standard treatment for many gynecologic, genitourinary, and gastrointestinal malignancies consists of concurrent chemoradiotherapy, with or without adjuvant chemotherapy. Hematologic toxicity is an important limiting factor in the treatment of pelvic malignancies, as multiple studies have correlated reduced chemotherapy intensity with poorer treatment outcomes [1–4].

It is well-documented that radiation causes significant bone marrow (BM) injury, contributing to low peripheral blood cell counts and poor tolerance to chemotherapy [5–7]. Correspondingly, numerous studies have found that increased pelvic BM radiation dose is associated with increased hematologic toxicity, suggesting that techniques to reduce BM irradiation may be effective in improving chemotherapy delivery [8–15]. For example, intensity modulated radiation therapy (IMRT) is a modern technology that can reduce BM dose compared to conventional techniques, without compromising target coverage [16]. Much evidence suggests that IMRT is effective in reducing toxicity of chemoradiotherapy, though prospective randomized trials are lacking [17].

It has long been known that human BM is comprised of both hematopoietically active (“red”) and inactive fatty (“yellow”) subregions. Recent studies have indicated that radiation-induced BM toxicity appears to depend on dose specifically to metabolically active BM subregions [12,15]. Functional and quantitative imaging techniques have increasingly been used to identify active BM for image-guided BM-sparing IMRT (IG-BMS-IMRT) [12,15,18–20]. For example, positron emission tomography (PET) has been employed, with the most common radiopharmaceuticals being [^{18}F]Fluoro-2-deoxy-2-D-glucose (FDG) and 3′-deoxy-3′-[^{18}F]fluorothymidine (FLT). FDG accumulates in metabolically active cells, whereas FLT accumulates in proliferating cells [21]. However, it is unknown whether FDG and FLT agree or are consistent in identifying active BM, and which technique (if any) is optimal for use in IG-BMS-IMRT planning.

The aims of this study were 1) to quantify the extent of agreement between FDG-PET/CT and FLT-PET/CT in identifying active pelvic BM subregions, 2) to quantify individual variation in the relative location of active BM identified by FDG-PET/CT and FLT-PET/CT, and 3) to compare the distribution of FDG-defined versus FLT-defined active BM, and determine which is likely to be superior for IG-BMS-IMRT planning.

MATERIALS AND METHODS

Population and Sampling Methods

The University of California San Diego (UCSD) Institutional Review Board approved this study, and eligible patients provided written informed consent. We complied with the Health Insurance Portability and Accountability Act. We included cervical cancer patients enrolled

on one of three prospective clinical trials performed at UCSD. The first trial included 12 cervical cancer patients treated on a pilot study of IG-BMS-IMRT [20]. The second trial included 25 cervical cancer patients treated at UCSD on a multi-center phase II clinical trial of IMRT with concurrent cisplatin (clinicaltrials.gov identifier: NCT01554397). The third trial included 16 cervical cancer patients treated with IMRT and concurrent cisplatin and escalating doses of gemcitabine at UCSD on a phase I clinical trial (clinicaltrials.gov identifier: NCT01554410).

Eligible patients had International Federation of Gynecology and Obstetrics stage I-IVA histologically proven cervical carcinoma, with pre-treatment FDG-PET/CT and/or FLT-PET/CT, and no history of prior malignancy in the preceding three years (excluding non-melanomatous skin cancer), no history of prior pelvic radiotherapy or chemotherapy, and no history of hip, pelvic, or lumbosacral prosthesis or implanted device. Of 53 potentially eligible patients, 9 did not undergo PET/CT and 3 had imaging data that were unrecoverable, leaving 41 patients for analysis. Pre-treatment FDG-PET/CT and/or FLT-PET/CT were used for all analyzable patients.

PET/CT Imaging

Of the 41 subjects included in this study, 25 underwent pre-treatment FDG-PET/CT only, 7 underwent pre-treatment FLT-PET/CT only, and 9 underwent both pre-treatment FDG-PET/CT and FLT-PET/CT. FLT-PET/CT scans were funded by an NIH grant (R21CA162718-01) whereas FDG-PET/CT scans were funded by patients' insurers. Some patients refused to consent for the FLT study and some patients' insurers refused to cover FDG-PET/CT scans, which is why some patients had one or the other scan but not both. The median time between FDG-PET/CT and FLT-PET/CT in patients who had both scans was 29 days (range: 6–94).

All FLT-PET/CT and FDG-PET/CT scans were performed using a GE Medical Systems Discovery STE or LightSpeed model, and 48 of the 50 total PET scans were performed at UCSD with a 3.27 mm interslice distance. The UCSD scanner is registered with the American College of Radiology Imaging Network. The remaining 2 FDG-PET/CT scans (for patients with both modalities) were performed on non-registered non-UCSD scanners and had a 4.25 mm interslice distance. Patients imaged with FDG-PET underwent intravenous administration of 10–20 mCi of FDG one hour prior to imaging (actual mean activity: 615 ± 91 MBq (population standard deviation (PSD)), range: 460 – 786 MBq; actual mean time between FDG administration and simulation: 70 ± 15 minutes (PSD), range of 43 – 105 minutes). Patients imaged with FLT-PET underwent intravenous administration of 4.5 MBq/kg one hour prior to imaging (actual mean activity: 337 ± 80 MBq (PSD), range: 194 – 505 MBq; actual mean time between FLT administration and simulation: 71 ± 13 minutes (PSD), range of 55 – 96 minutes. Attenuation correction was performed with a low dose CT acquisition. All PET corresponding CT images had a 2.5 mm interslice distance except for 2 patients with a 3.75 mm interslice distance, 1 with a 4.25 mm interslice distance, and 1 with a 5 mm interslice distance. The planning CTs for all patients had a 2.5 mm interslice distance and were performed using either GE Medical Systems Discovery STE or LightSpeed models.

Image Registration and Segmentation Methods

For patients with both FDG-PET and FLT-PET scans, the corresponding CT image was deformably co-registered to the patient's planning (simulation) CT using Velocity AI software (Velocity Medical Solutions, Atlanta, GA), only registering between the superior border of the L5 vertebral body and the inferior border of the ischial tuberosities. The co-registered PET images were then resampled to match the voxel dimensions of the planning CT.

Pelvic BM was contoured on the planning CT and defined as the L5 vertebral body, os coxae, entire sacrum, coccyx, and proximal femora cut at the level defined by the most caudal point of the ischial tuberosities. The active BM subvolume was defined as a subset of the pelvic BM with standardized uptake values corrected for body weight (SUV) above a designated threshold. Three SUV thresholds were chosen for each PET image such that they defined an active BM subvolume comprising 40%, 50%, and 60% of the total pelvic BM volume in order to compare volumes of equal size. Previous studies using PET images to identify active BM have used SUV above mean pelvic SUV to define active BM [12,15,20]. This choice is arbitrary and further research is needed to determine an optimal cutoff. We chose 40%, 50%, and 60% of the total pelvic BM volume because we have found that using SUV above the mean pelvic SUV usually produces a volume within this range. Although the choice of active BM cutoff is also somewhat arbitrary, our goal was to experiment within a range of BM volumes that were large enough to be clinically meaningful, but small enough to be feasible to spare. At extreme values of the relative subvolume, the analysis becomes trivial because the subvolume is either too small to be clinically meaningful, or too large to have a meaningful difference between the subvolume and the total volume. In addition, by making the active BM a percentage of the total pelvic volume, the comparison of FDG and FLT is more intuitive because the Dice coefficient can be thought of as a percent overlap when the size of the volumes compared is exactly the same.

The Dice similarity coefficient, or "Dice coefficient", was computed for each of the three active BM subvolumes created from both FDG and FLT scans for each patient. The Dice coefficient equals the percent overlap of two volumes (when they are of equal size) and is a measure of the similarity in volumes defined by FDG-PET and FLT-PET. Perfect overlap yields a Dice coefficient value of 100%, whereas no overlap yields value of 0%. It is calculated as follows:

$$\text{Dice coefficient} = \frac{2 \cdot \mathrm{N}(\mathrm{A} \cap \mathrm{B})}{\mathrm{N}(\mathrm{A}) + \mathrm{N}(\mathrm{B})}$$

where N(A∩B) is the number of elements that intersect between set A and set B, N(A) is the number of elements in set A, and N(B) is the number of elements in set B [22].

We selected one planning CT as a canonical template from a patient with both FDG-PET and FLT-PET scans, whose pelvic BM volume was closest to the median pelvic BM volume of all patients in the study. Average images were created by deformably co-registering the corresponding CT images to the canonical template and resampling the co-registered PET

images to match the template voxel dimensions. The deformed and resampled images were normalized and then averaged to create two sets of average FDG-PET and FLT-PET images: one for all of the patients that had both scans, and another for all available patients. We calculated Dice coefficients to quantify the similarity in the active BM defined by these average images for 40%, 50%, and 60% volume thresholds. To quantify individual variability in the location of active BM, we also calculated Dice coefficients for each individual's active BM subvolumes using the co-registered deformed images compared with the subvolumes produced by the average image using all of the available patients.

Method for Comparing FDG and FLT Active BM Distributions

We implemented a region-growing algorithm to quantify the differences in the distribution of active BM defined by FDG-PET and FLT-PET. The initial starting point/seed point of the region-growing algorithm was the entire active BM subvolume, then the active BM volume was expanded in an iterative fashion such that during each iteration, non-active voxels directly adjacent to the active BM became part of the updated active BM volume for the next iteration. This process repeated until the active BM volume expanded to fill the total pelvic BM volume. The region-growing algorithm considered each active voxel to have 26 neighbors (6 sharing a face, 12 sharing an edge, and 8 sharing a vertex) into which the volume could potentially expand [23]. Fewer iterations indicates a more dispersed active BM subvolume, which is theoretically more difficult to spare during conformal radiation therapy (such as IMRT). This concept is illustrated schematically in Figure 1, showing two hypothetical pelvises with different active BM distributions represented by red pixels. Qualitatively, Pelvis 1 has an active BM subregion that is more diffuse and difficult to spare than Pelvis 2. This is quantitatively reflected in the region-growing results: it takes one iteration to completely expand the active BM subregion in Pelvis 1, but three iterations to completely expand the active BM subregion in Pelvis 2. Using this method we were able to quantitatively and reproducibly compare differences in three-dimensional active BM volume distributions. Figure 2 illustrates the region-growing algorithm performed on the average FLT image for all patients in our sample, with successive iterations labeled and colored progressively from red to yellow.

Statistical Methods

Confidence intervals were estimated using the t-distribution. Continuous measures were compared within subgroups using analysis of variance. Categorical measures were compared within subgroups using chi-square tests. All statistical tests were two-sided with $p < 0.05$ indicating statistical significance.

RESULTS

Sample Description

Sample characteristics are presented in Table 1. Notably, the mean age ($p=0.41$) and pelvic BM volumes ($p = 0.07$) were not significantly different in patients with FDG-PET only, versus FLT-PET only, versus patients co-imaged with FDG-PET and FLT-PET. Race, stage, histology, and grade were also not significantly different across subgroups.

Agreement Between FLT and FDG Active BM Subvolumes

For patients with both modalities, the mean Dice coefficients ± 95% confidence interval for the 40%, 50%, and 60% subvolumes were 0.683±0.029 (0.606–0.725), 0.732±0.021 (0.676–0.768), and 0.781±0.014 (0.745–0.807) respectively (minimum-maximum). Dice coefficients comparing the 40%, 50%, and 60% active BM contours from average images using only patients with both modalities were 0.758, 0.796, and 0.828 respectively, whereas Dice coefficients of subvolumes from average images using all of the patients were 0.773, 0.805, and 0.839 respectively. The mean SUVs ± 95% confidence interval for all of the FDG scans were 1.04±0.096, 0.95±0.086, and 0.88±0.078 for the 40%, 50%, and 60% thresholds respectively. The same data for the FLT scans were 2.93±0.46, 2.47±0.38, 2.08±0.31 respectively. However, as others have noted, one should exercise caution when comparing SUVs among different patients [24]. In addition, two of the FDG scans for patients with both modalities were done at non-UCSD facilities and thus we cannot assure cross calibration. We did not observe any significant correlations between Dice coefficients and activity of FLT or FDG delivered or time between injection and image acquisition.

Comparison of FDG and FLT Variability

We further calculated Dice coefficients between the individual FDG-based active BM volume and the average FDG-based active BM volume, for all 34 patients imaged with FDG-PET (Table 2). We repeated the same calculation for all 16 patients imaged with FLT-PET (Table 2). These coefficients quantify the individual variability in the location of active BM. Figure 3 shows histograms of the FDG-PET and FLT-PET Dice coefficients comparing individual vs. average image active BM volumes, according to the threshold used to define the subvolume. Figure 4 shows the representative (average) active BM contours using all of the patients for the three thresholds.

Comparison of FDG and FLT Distributions

The mean differences in iterations (FLT iterations minus FDG iterations) using the region-growing algorithm for the 40%, 50%, 60% subvolumes were 11.3 (6.8, 0.001, 1–23), 14.2 (5.9, <0.001, 7–26), and 14.0 (7.1, <0.001, 2–26) respectively (sample standard deviation, p-value, minimum-maximum). The respective iteration differences for the subvolumes from the average image using patients with both modalities were 1, 3, and 6, whereas the same data for the average image using all patients are 2, 2, and 4 respectively. These findings indicate a significantly higher number of iterations for FLT-PET, suggesting that, for the same size volume, the FLT-defined active BM is more concentrated, less diffuse, and thus easier to spare using conformal radiotherapy planning techniques such as IMRT.

DISCUSSION

BM-sparing IMRT is a promising treatment that may reduce hematologic toxicity and permit better tolerance to concurrent, adjuvant, and/or salvage chemotherapy for a variety of pelvic malignancies. Although multiple lines of evidence support the hypothesis that reducing radiation dose to pelvic BM, particularly functional BM subregions, is likely to be effective, this approach remains investigational. Barriers to the use of IG-BMS-IMRT

include its higher cost and complexity, and paucity of prospective controlled evidence of its benefits relative to standard radiotherapy techniques.

Among the basic unanswered questions about IG-BMS-IMRT are which quantitative imaging technique(s), if any, should be used to identify the BM subregions for sparing, and how this information should be used specifically. A variety of methods have been investigated, including Tc-99m sulfur colloid single photon emission computed tomography (SPECT) [18], FLT-PET [19], FDG-PET [12,15,20], and quantitative magnetic resonance imaging (MRI) [20]. FLT-PET is often assumed to be the best available method for functional BM imaging, however, few studies have directly compared alternative BM imaging techniques or formally quantified their differences. Compared to FDG, FLT is not as commonly available and is more expensive, which is why it would be important to know whether FDG can serve the clinical purpose as a reasonable and cost-effective substitute for FLT.

This study compares alternative BM imaging approaches for the purpose of guiding radiotherapy planning. Although we found significant overlap between FLT-PET and FDG-PET, FLT-PET is likely superior for BM-sparing strategies, by virtue of its higher inter-patient consistency and tendency to identify a more highly concentrated BM subvolume. These findings add to evidence supporting FLT-PET over FDG-PET in treatment planning and assessing BM impairment outside of the radiotherapy field [25–26]. In addition, the higher inter-patient consistency makes FLT-PET potentially more attractive for creating class solutions to define population-wide active BM regions for use when PET is unavailable [27]. However, FDG-PET-guided and FLT-PET-guided radiotherapy approaches remain potential strategies for both BM sparing and target delineation [25,28–29].

A strength of this study was its homogeneous sample drawn from subjects with cervical cancer participating in prospective clinical trials, 9 of whom were co-imaged with FLT-PET and FDG-PET prior to treatment. The results, however, should be interpreted with caution, given the limited sample size, and might not be applicable to other pelvic malignancies or males. Uncertainty in localization of active BM due to insufficient spatial resolution, image co-registration errors, and daily setup errors are also factors that may limit the effectiveness of IG-BMS-IMRT. Nonetheless, ongoing prospective multi-center trials are testing the effectiveness of BM-sparing IMRT and should lend insight into the potential of this treatment approach.

Acknowledgments

The project was supported by the National Institutes of Health Grants R21CA162718-01 and T35 AG026757/AG/NIA, and the University of California, San Diego, Stein Institute for Research on Aging. The sponsors had no involvement in the study design, collection/analysis/interpretation of the data, writing of the manuscript, or decision to submit the manuscript for publication.

References

1. Peters WA 3rd, Liu PY, Barrett RJ 2nd, et al. Concurrent chemotherapy and pelvic radiation therapy compared with pelvic radiation therapy alone as adjuvant therapy after radical surgery in high-risk early-stage cancer of the cervix. J Clin Oncol. 2000; 18:1606–13. [PubMed: 10764420]
2. Nugent EK, Case AS, Hoff JT, et al. Chemoradiation in locally advanced cervical carcinoma: an analysis of cisplatin dosing and other clinical prognostic factors. Gynecol Oncol. 2010; 116:438–41. [PubMed: 19896180]
3. Dueñas-Gonzalez A, Cetina-Perez L, Lopez-Graniel C, et al. Pathologic response and toxicity assessment of chemoradiotherapy with cisplatin versus cisplatin plus gemcitabine in cervical cancer: a randomized Phase II study. Int J Radiat Oncol Biol Phys. 2005; 61:817–23. [PubMed: 15708261]
4. Dueñas-González A, Zarbá JJ, Patel F, et al. Phase III, open-label, randomized study comparing concurrent gemcitabine plus cisplatin and radiation followed by adjuvant gemcitabine and cisplatin versus concurrent cisplatin and radiation in patients with stage IIB to IVA carcinoma of the cervix. J Clin Oncol. 2011; 29:1678–85. [PubMed: 21444871]
5. Mauch P, Constine L, Greenberger J, et al. Hematopoietic stem cell compartment: acute and late effects of radiation therapy and chemotherapy. Int J Radiat Oncol Biol Phys. 1995; 31:1319–39. [PubMed: 7713791]
6. Fajardo, LF.; Berthrong, M.; Anderson, RE. Hematopoietic tissue. In: Fajardo, LF.; Berthrong, M.; Anderson, RE., editors. Radiation pathology. Oxford: Oxford University Press; 2001. p. 379-88.
7. Hall, EJ.; Giaccia, AJ. Clinical response of normal tissues. In: Hall, EJ.; Giaccia, AJ., editors. Radiobiology for the radiologist. 6. Philadelphia: Lippincott Williams & Wilkins; 2006. p. 333-337.p. 461-62.
8. Brixey CJ, Roeske JC, Lujan AE, Yamada SD, Rotmensch J, Mundt AJ. Impact of intensity modulated radiotherapy on acute hematologic toxicity in women with gynecologic malignancies. Int J Radiat Oncol Biol Phys. 2002; 54:1388–96. [PubMed: 12459361]
9. Mell LK, Kochanski JD, Roeske JC, et al. Dosimetric predictors of acute hematologic toxicity in cervical cancer patients treated with concurrent cisplatin and intensity-modulated pelvic radiotherapy. Int J Radiat Oncol Biol Phys. 2006; 66:1356–65. [PubMed: 16757127]
10. Mell LK, Schomas DA, Salama JK, et al. Association between bone marrow dosimetric parameters and acute hematologic toxicity in anal cancer patients treated with concurrent chemotherapy and intensity-modulated radiotherapy. Int J Radiat Oncol Biol Phys. 2008; 70:1431–37. [PubMed: 17996390]
11. Rose BS, Aydogan B, Liang Y, et al. Normal tissue complication probability modeling of acute hematologic toxicity in cervical cancer patients treated with chemoradiotherapy. Int J Radiat Oncol Biol Phys. 2011; 79:800–07. [PubMed: 20400238]
12. Rose BS, Liang Y, Lau SK, et al. Correlation between radiation dose to ^{18}F-FDG-PET defined active bone marrow subregions and acute hematologic toxicity in cervical cancer patients treated with chemoradiotherapy. Int J Radiat Oncol Biol Phys. 2012; 83:1185–91. [PubMed: 22270171]
13. Klopp AH, Moughan J, Portelance L, et al. Hematologic toxicity in RTOG 0418: a phase 2 study of postoperative IMRT for gynecologic cancer. Int J Radiat Oncol Biol Phys. 2013; 86:83–90. [PubMed: 23582248]
14. Carmona R, Pritz J, Bydder M, et al. Fat composition changes in bone marrow during chemotherapy and radiation therapy. Int J Radiat Oncol Biol Phys. 2014; 90:155–63. [PubMed: 25015207]
15. Elicin O, Callaway S, Prior JO, Bourhis J, Ozsahin M, Herrera FG. [(18)F]FDG-PET standard uptake value as a metabolic predictor of bone marrow response to radiation: impact on acute and late hematological toxicity in cervical cancer patients treated with chemoradiation therapy. Int J Radiat Oncol Biol Phys. 2014; 90:1099–1107. [PubMed: 25442041]
16. Mell LK, Tiryaki H, Ahn KH, Mundt AJ, Roeske JC, Aydogan B. Dosimetric comparison of bone marrow-sparing intensity-modulated radiotherapy versus conventional techniques for treatment of cervical cancer. Int J Radiat Oncol Biol Phys. 2008; 71:1504–10. [PubMed: 18640499]

17. Mell LK. Intensity modulated radiation therapy for gynecologic malignancies: a testable hypothesis. Int J Radiat Oncol Biol Phys. 2012; 84:566–68. [PubMed: 22999264]
18. Roeske JC, Lujan A, Reba RC, Penney BC, Yamada SD, Mundt AJ. Incorporation of SPECT bone marrow imaging into intensity modulated whole-pelvic radiation therapy treatment planning for gynecologic malignancies. Radiother Oncol. 2005; 77:11–17. [PubMed: 16024116]
19. McGuire SM, Menda Y, Boles Ponto LL, Gross B, Juweid M, Bayouth JE. A methodology for incorporating functional bone marrow sparing in IMRT planning for pelvic radiation therapy. Radiother Oncol. 2011; 99:49–54. [PubMed: 21397965]
20. Liang Y, Bydder M, Yashar CM, et al. Prospective study of functional bone marrow-sparing intensity modulated radiation therapy with concurrent chemotherapy for pelvic malignancies. Int J Radiat Oncol Biol Phys. 2013; 85:406–14. [PubMed: 22687195]
21. Everitt SJ, Ball DL, Hicks RJ, et al. Differential ^{18}F-FDG and ^{18}F-FLT uptake on serial PET/CT imaging before and during definitive chemoradiation for non-small cell lung cancer. J Nucl Med. 2014; 55:1069–74. [PubMed: 24833494]
22. Hanna GG, van Sörnsen de Koste JR, Dahele MR, et al. Defining target volumes for stereotactic ablative radiotherapy of early-stage lung tumours: a comparison of three-dimensional 18F-fluorodeoxyglucose positron emission tomography and four-dimensional computed tomography. Clin Oncol (R Coll Radiol). 2012; 24:e71–e80. [PubMed: 22445302]
23. Lu Y, Jiang T, Zang Y. Region growing method for the analysis of functional MRI data. Neuroimage. 2003; 20:455–65. [PubMed: 14527606]
24. Keyes JW Jr. SUV: Standard uptake or silly useless value? J Nucl Med. 1995; 36:1836–1839. [PubMed: 7562051]
25. Han D, Yu J, Yu Y, et al. Comparison of (18)F-fluorothymidine and (18)F-fluorodeoxyglucose PET/CT in delineating gross tumor volume by optimal threshold in patients with squamous cell carcinoma of thoracic esophagus. Int J Radiat Oncol Biol Phys. 2010; 76:1235–41. [PubMed: 19910143]
26. Leimgruber A, Möller A, Everitt SJ, et al. Effect of platinum-based chemoradiotherapy on cellular proliferation in bone marrow and spleen, estimated by ^{18}F-FLT PET/CT in patients with locally advanced non-small cell lung cancer. J Nucl Med. 2014; 55:1075–80. [PubMed: 24868108]
27. McGuire SM, Menda Y, Boles Ponto LL, et al. Spatial mapping of functional pelvic bone marrow using FLT PET. J Appl Clin Med Phys. 2014; 15:4780. [PubMed: 25207403]
28. Herrera FG, Prior JO. The role of PET/CT in cervical cancer. Front Oncol. 2013; 3:34, 1–10. [PubMed: 23549376]
29. Patel DA, Chang ST, Goodman KA, et al. Impact of integrated PET/CT on variability of target volume delineation in rectal cancer. Technol Cancer Res Treat. 2007; 6:31–36. [PubMed: 17241098]

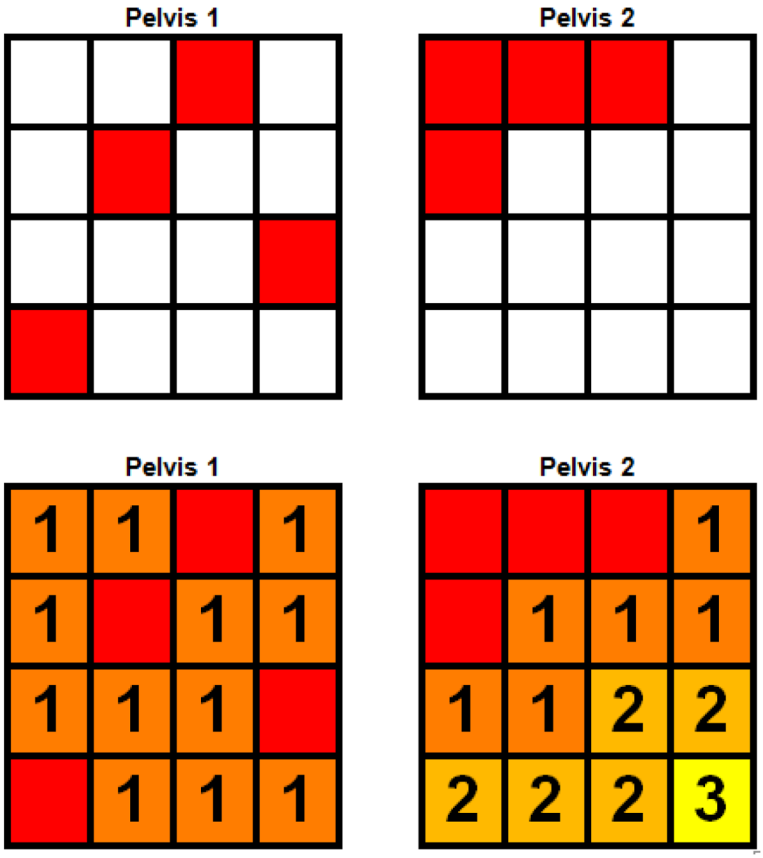

Figure 1.

Schema of region-growing algorithm. The top two grids represent hypothetical pelvises with different distributions of active BM, represented by red pixels. The bottom two grids depict region-growing performed on the active BM with successive iterations labeled by numbers and colored progressively from red to yellow. The active BM distribution for Pelvis 2 is more concentrated and would be more amenable for sparing with conformal radiotherapy than Pelvis 1, and correspondingly has a higher number of iterations to fill the grid.

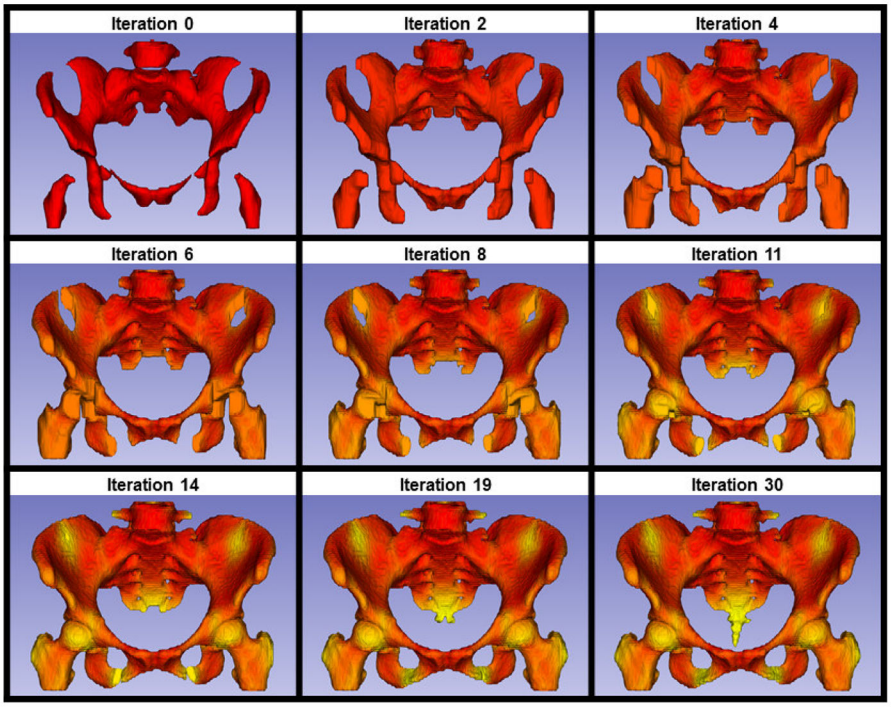

Figure 2.

Progressive iterations (labeled above each image) of the region-growing algorithm performed on a 50% active BM subvolume. This subvolume was derived from the average image of all FLT patients. The active BM subvolume begins as red and subsequent voxels added in successive iterations slowly transition from red to yellow.

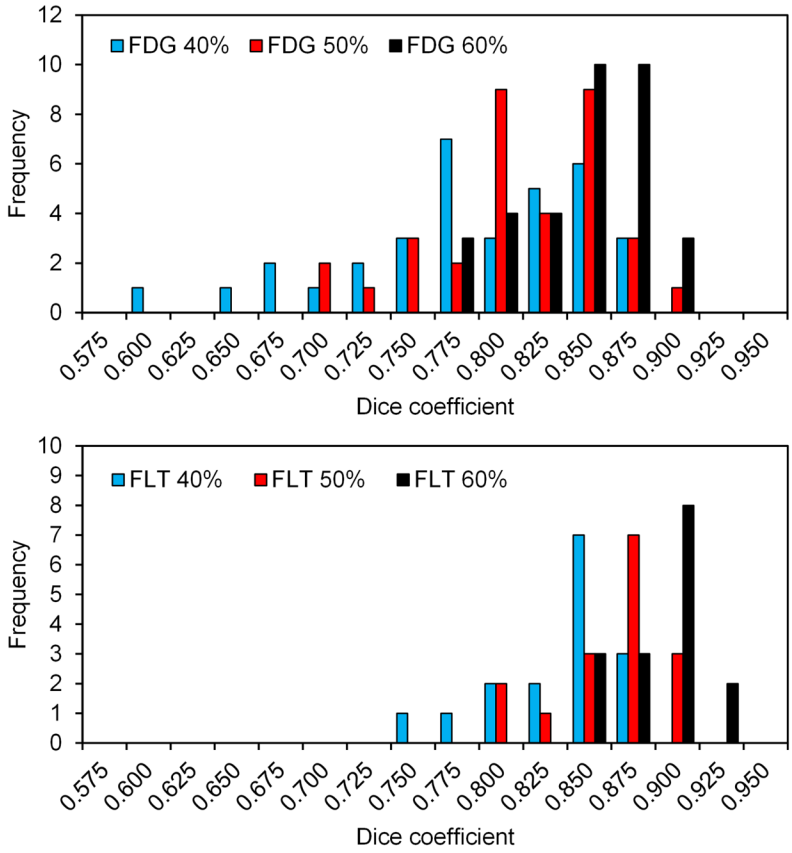

Figure 3.

The top histogram shows the distribution of Dice coefficients comparing the active BM defined using FDG (n=34) to the active BM created from the average FDG image for the 40%, 50%, and 60% thresholds. The bottom histogram shows the same information on the same scale for FLT (n=16).

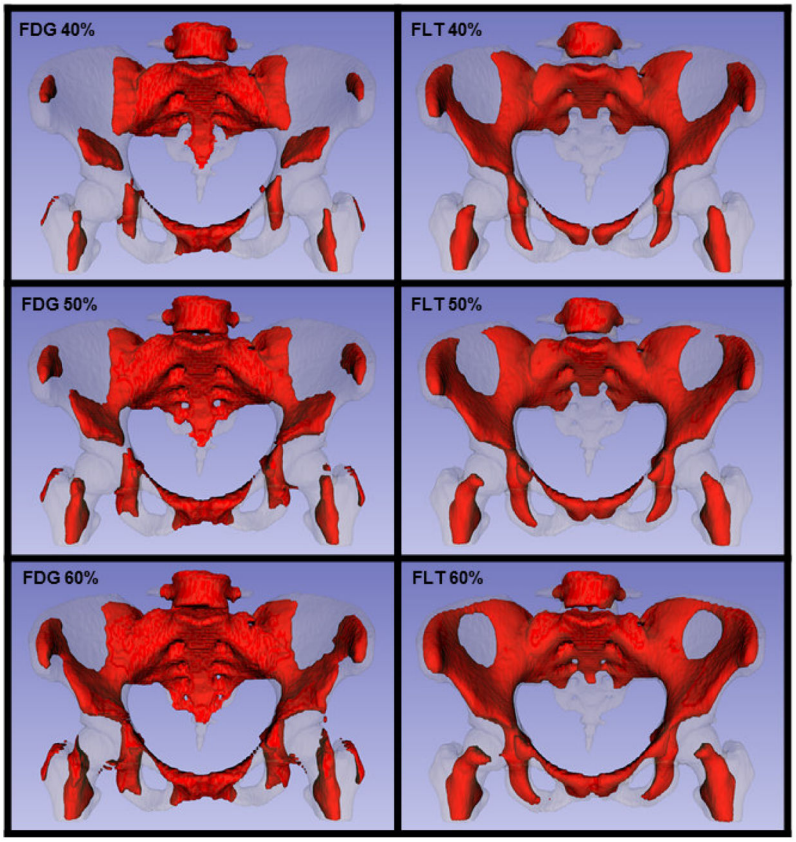

Figure 4.
Rendering of active BM contours at 40%, 50%, and 60% thresholds from the average FDG (n=34) and FLT (n=16) images.

Table 1

Sample Characteristics

Characteristic	All	FDG Only	FLT Only	FDG & FLT	p
Number of patients	41	25	7	9	
Mean age, years (SD)	50 (13)	48 (11)	56 (16)	49 (130	0.41
Age range, years	26–83	26–70	41–83	35–65	
Race, n (%)					
Caucasian	18 (44%)	8 (32%)	4 (57%)	6 (67%)	0.15
Hispanic	16 (39%)	13 (52%)	2 (29%)	1 (11%)	0.08
African-American	2 (5%)	2 (8%)	0 (0%)	0 (0%)	0.99
Asian	3 (7%)	1 (4%)	1 (14%)	1 (11%)	0.33
Other	2 (5%)	1 (4%)	0 (0%)	1 (11%)	0.63
FIGO stage, n (%)					
IB	11 (27%)	7 (28%)	1 (14%)	3 (33%)	0.85
IIA	1 (2%)	0 (0%)	1 (14%)	0 (0%)	0.17
IIB	14 (34%)	6 (24%)	3 (43%)	5 (56%)	0.19
IIIB	12 (29%)	9 (36%)	2 (29%)	1 (11%)	0.39
IVA	2 (5%)	2 (8%)	0 (0%)	0 (0%)	0.99
Recurrent	1 (2%)	1 (4%)	0 (0%)	0 (0%)	0.99
Histology, n (%)					
Squamous	27 (66%)	17 (68%)	4 (57%)	6 (67%)	0.90
Adenocarcinoma	12 (29%)	6 (24%)	3 (43%)	3 (33%)	0.34
Adenosquamous Carcinoma	2 (5%)	2 (8%)	0 (0%)	0 (0%)	0.99
Grade, n (%)					
2	11 (27%)	5 (20%)	3 (43%)	3 (33%)	0.48
3	18 (44%)	13 (52%)	4 (57%)	1 (11%)	0.09
Not reported	12 (29%)	7 (28%)	0 (0%)	5 (56%)	0.06
Mean pelvic BM volume, cm^3 (SD)	1122 (155)	1080 (166)	1146 (136)	1217 (84)	0.07
Pelvic BM volume range, cm^3	721–1403	721–1388	966–1404	1085–1307	

Abbreviations: FDG, [^{18}F]fluorodeoxyglucose; FLT, [^{18}F]fluorothymidine; SD, sample standard deviation; n, number; FIGO, International Federation of Gynecologic Oncology; BM, bone marrow.

Table 2

Individual vs. Average Active BM Dice Coefficients

Category	Minimum	Maximum	Median	SD	Mean ± 95% CI
40% FDG	0.598	0.872	0.781	0.067	0.773 ± 0.023
40% FLT	0.739	0.873	0.835	0.038	0.825 ± 0.020
50% FDG	0.683	0.877	0.803	0.050	0.801 ± 0.017
50% FLT	0.787	0.895	0.859	0.031	0.852 ± 0.017
60% FDG	0.752	0.889	0.834	0.036	0.832 ± 0.013
60% FLT	0.825	0.912	0.885	0.024	0.877 ± 0.013

Abbreviations: FDG, [^{18}F]fluorodeoxyglucose; FLT, [^{18}F]fluorothymidine; SD, sample standard deviation; CI, confidence interval; BM, bone marrow.